NANO LETTERS

Letter

pubs.acs.org/NanoLett

Nanoscale Fluorescence Lifetime Imaging of an Optical Antenna with a Single Diamond NV Center

Ryan Beams,[†] Dallas Smith,[†] Timothy W. Johnson,[‡] Sang-Hyun Oh,[‡] Lukas Novotny,[§] and A. Nick Vamivakas*,[†]

[†]Institute of Optics, University of Rochester, Rochester, New York 14627, United States

[‡]Department of Electrical and Computer Engineering, University of Minnesota, Minneapolis, Minnesota 55455, United States

[§]ETH Zürich, Photonics Laboratory, 8093 Zürich, Switzerland

Supporting Information

ABSTRACT: Solid-state quantum emitters, such as artificially engineered quantum dots or naturally occurring defects in solids, are being investigated for applications ranging from quantum information science and optoelectronics to biomedical imaging. Recently, these same systems have also been studied from the perspective of nanoscale metrology. In this letter, we study the near-field optical properties of a diamond nanocrystal hosting a single nitrogen vacancy center. We find that the nitrogen vacancy center is a sensitive probe of the surrounding electromagnetic mode structure. We exploit this sensitivity to demonstrate nanoscale fluorescence lifetime imaging microscopy (FLIM) with a single nitrogen vacancy center by imaging the local density of states of an optical antenna.

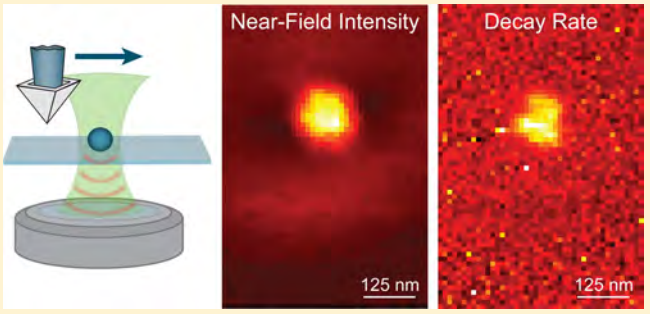

KEYWORDS: *Near-field scanning optical microscopy, NV center, fluorescence lifetime imaging, local density of optical states, optical antenna*

Controlled interaction of light and matter at the nanoscale requires a detailed understanding of the local electromagnetic mode distribution. It has been recognized for some time that, in contrast to the homogeneity exhibited by the vacuum electromagnetic modes in free space, surfaces and nanostructured environments can sculpt the local electromagnetic mode density or local density of optical states (LDOS). A manifestation of this modification, as first pointed out by Purcell,[1] is that the excited state lifetime of a quantum object is not an immutable property, but depends sensitively on the system's environment. Since the pioneering experiments of Drexhage[2] and Kleppner,[3] numerous demonstrations have illustrated the impact LDOS engineering has on excited state decay dynamics through plasmonics,[4−10] cavities,[11,12] or other means.[13−15] Apart from a deeper understanding of how matter exchanges energy with the electromagnetic field, a detailed understanding of the LDOS is technologically relevant as photonic devices continue to shrink to the nanoscale.[16]

One approach to LDOS mapping utilizes the excited state lifetime of an optically active material as a monitor of the local electromagnetic environment.[17,18] During the past decade there has been a continued effort toward the realization of nanoscale fluorescence lifetime imaging microscopy (FLIM) with a single quantum system.[19−25] One system being explored for this application is the nitrogen vacancy center (NV center) in diamond.[26] NV centers have already found numerous applications ranging from quantum information science,[27] single-photon generation,[28,29] and quantum metrology[30−36] to fluorescence-based bioimaging.[37] Initial single emitter FLIM measurements used single molecules[8] and quantum dots.[9] However, these emitters suffer from fluorescence bleaching and blinking. Important for the present work is that the NV center exhibits stable photoluminescence at room temperature, and the center's optical properties are preserved when the diamond host takes the form of a nanocrystal. In the following, we exploit the previous features to demonstrate nanoscale FLIM of a nanoscale optical antenna[38] with a single NV center.

The top panel of Figure 1a presents an illustration of the FLIM concept. In the first modality a single quantum system (the probe) is affixed to the vertex of a nanoscale tip and a sample to be interrogated (the object) is scanned in close proximity to the emitter. The object perturbs the local environment of the probe and modifies its excited state dynamics that can be recorded as a function of the object's $x-y$ coordinates to build an image. A second approach, followed in the present work, is to fix the probe in space (see bottom panel of Figure 1a) and scan the object through the focus. Again, by monitoring the probe lifetime, an image can be recorded. In our

Received: May 16, 2013
Revised: June 24, 2013
Published: July 1, 2013

 © 2013 American Chemical Society dx.doi.org/10.1021/nl401791v | *Nano Lett.* 2013, 13, 3807−3811

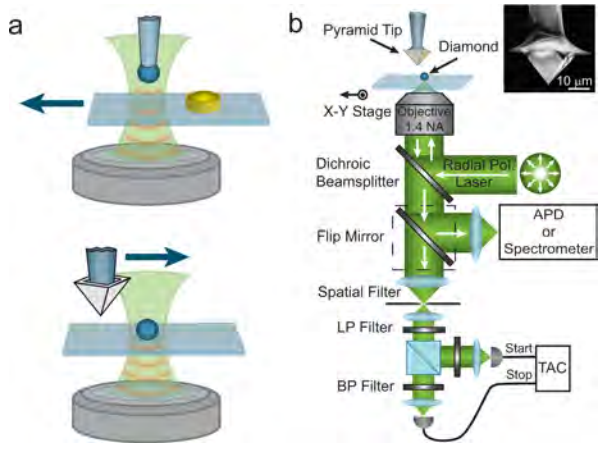

Figure 1. Concept and experimental setup. (a) Top panel: Fluorescence lifetime imaging microscopy with a scanning quantum system. A target object is fixed in space, and the probe quantum system is scanned in the vicinity of the target. The probe lifetime is recorded as a function of its position to build an image. Bottom panel: The probe is fixed in space, and the target object is scanned in the vicinity of the probe to build a lifetime image. (b) An inverted confocal microscope is combined with a homemade AFM scan head. The excitation beam polarization can be prepared in linear or radial polarization. The resultant fluorescence is spectrally resolved, collected by an APD for lifetime and fluorescence images, or sent to a pair of APDs for intensity autocorrelation measurements. LP = long pass filter. BP = bandpass filter. TAC = time to amplitude converter. Inset: SEM image of an Ag pyramid (tip 1 in the text).

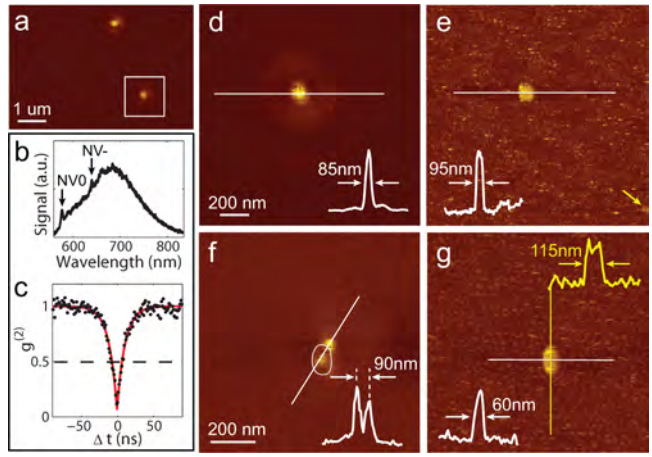

Figure 2. Near-field optics of a single nitrogen vacancy. (a) Scanning confocal fluorescence image of NV centers under radial excitation. The white square denotes NV center 1. (b) Spectrum of NV center 1. The zero phonon lines (ZPL) for the two charged states are indicated. (c) Intensity autocorrelation function of the fluorescence for NV center 1. There is no background correction. (d) The near-field fluorescence image of NV center 1 with a Ag pyramid tip (tip 1). Inset: Linecut corresponding to the line indicated in the image. (e) Topography map for NV center 1 with tip 1 taken simultaneously to the near-field image. Crystal height is ~20 nm. Arrow indicates small feature 10 nm high. Inset: Linecut corresponding to the line indicated in the image. (f) The near-field fluorescence image of NV center 1 with a second Ag pyramid tip (tip 2). Inset: Linecut corresponding to the line indicated in the image. (g) Topography map for NV center 1 with tip 2 taken simultaneously to the near-field image. Crystal height is ~20 nm. Inset: Linecut corresponding to the line indicated in the image.

experiments, a single NV center in a diamond nanocrystal is our probe of the nanoscale LDOS created by the object.

Figure 1b presents a schematic of our experimental setup. A solution of diamond nanocrystals (Academia Sinica/Adamas) is sonicated and spin-cast onto a glass coverslip, which is then mounted on a scanning $x-y$ piezo stage in the focus of an inverted confocal microscope. The objective numerical aperture is 1.4. On top of the sample stage is a home-built AFM scan head that incorporates a silver (Ag) tip in the geometry of a pyramid (inset Figure 1b). The Ag tips were prepared as in ref 39 with an additional photolithography step. To avoid oxidation, the Ag tips were kept in their silicon template until just before use. The tip can be scanned independently of the sample in $x-y-z$. Either a continuous wave (Coherent Compass) or pulsed (Picoquant) 532 nm light source was used to excite the NV center. Prior to the objective, the excitation beam is prepared in either radial or linear polarization. The resultant fluorescence is directed to a spectrometer, a single avalanche photodiode (APD) for imaging (both far- and near-field fluorescence images) and lifetime measurements, or to a pair of APDs for measurement of the intensity autocorrelation function (ORTEC nuclear instrument modules). All measurements reported are done well below the saturation power of the NV center with the Ag tip contributing a background of ~4000 cps (see Supporting Information Figure S5).

A far-field scanning confocal fluorescence image under radially polarized illumination is presented in Figure 2a. Radial polarization optimizes the near-field excitation of the NV center in the presence of the Ag tip. The spectrum in Figure 2b corresponds to the location outlined with the white square in the confocal image. From this spectrum, it is clear that both the neutral charged (NV^0) and negatively charged states (NV^-) are present. However, we selected out the NV^- state by placing a 645 nm long-pass filter in front of the APD used for near-field and FLIM imaging. A measurement of the intensity autocorrelation function determines if the diamond nanocrystal hosts a single NV center. Figure 2c presents an exemplary autocorrelation function, without background subtraction, for the same NV center outlined in Figure 2a. After determining a diamond nanocrystal hosts a single NV center, the Ag tip was aligned to the confocal focus. The NV center was scanned through the Ag tip-focus region, while fluorescence counts were recorded by the APD to construct a near-field image of the single NV center; previous studies have looked at nanodiamonds containing multiple NV centers.[24] Figure 2d,f presents near-field images of the same NV outlined in Figure 2a (NV1) with 2 different Ag tips (tip 1 and tip 2). The corresponding topography maps, shown in Figure 2e,g, allow us to determine the crystal heights to be ~20 nm (the feature indicated by the arrow in Figure 2e has a height of 10 nm). Shown as insets in both the near-field image and topography maps are linecuts along the direction indicated by the solid line. For the near-field image in Figure 2d (Figure 2f), we observe a fluorescence enhancement of 10 (7). In all crystals studied we measured on average an order of magnitude fluorescence enhancement (9.7 ± 2.6). Not included in this average is the maximum fluorescence enhancement we observed, which was ~17 (see Supporting Information Figure S1).

In comparing the two near-field images in Figure 2, the most salient feature is the localized fluorescence spots in Figure 2f. From the linecuts in Figure 2d,e, we observe that the homogeneous fluorescence exhibits the same subdiffraction limited width (full width at half-maximum (fwhm) of ~90 nm)

dx.doi.org/10.1021/nl401791v | Nano Lett. 2013, 13, 3807−3811

as the crystal's topography. This should be contrasted with Figure 2f where the fluorescence map exhibits localized hot spots (local increases in fluorescence counts) separated by ~90 nm with each feature revealing a subdiffraction limited width of 50 nm. This was not unique to this particular crystal-tip configuration (NV1/tip 2) or excitation polarization. We observed local hot-spots on a number of other single-NV center containing nanodiamonds with different tips for both radial and linear polarization (see Supporting Information Figure S3 for another near-field image with hot-spots).

A recent theoretical work modeled optically excited NV centers in a host diamond crystal.[40] This work showed that the diamond nanocrystal acts as a dielectric antenna that homogenizes the incident field inside the crystal and limits the maximum resolution of far-field measurement techniques to the size of the diamond nanocrystal.[37,41] The comparable resolution of the near-field fluorescence and topography in Figure 2c,d is in agreement with this theory. However, the hot spots in Figure 2f seem to be in conflict with this model.

There are several possible explanations that could resolve this inconsistency. For example, a double tip would manifest itself as two locations of increased fluorescence in the near-field image. We rule this out since the corresponding topography map (Figure 2f) does not exhibit a similar inhomogeneity (the outline of the crystal topography is the closed white curve in Figure 2f). The vertical cross-section through Figure 2g (yellow inset) shows a small topographic bump on top of the crystal. However, this was not present in the reverse scan-direction and is likely due to noise in the feedback-loop. A second cause is that for certain tip-crystal positions more light is scattered by the tip to the bucket APD detector. To eliminate this possibility, we performed lifetime linecuts across the diamond and observed that the total decay rate is locally increased at the hot spots (see Supporting Information Figure S4). This indicates that the excited state dynamics at the hot spots are different.

An alternative explanation is that the diamond nanocrystal and tip behaves as a dielectric and a metallic antenna. The appearance of the local hot spots then is a manifestation of specific tip-crystal configurations in which the combined effect of the tip and crystal antennas is to increase the LDOS and decrease the transition lifetime. These arrangements depend on the exact geometry of the tip and crystal, and the same crystal will interact differently with tips exhibiting different geometries. This argument can be framed exactly in terms of the partial LDOS (pLDOS), where the pLDOS is the electromagnetic mode density projected onto a particular dipole orientation. Mathematically, the pLDOS can be expressed as

$$\text{pLDOS} \propto [\hat{\mathbf{n}}\cdot\text{Im}\{G(\mathbf{r}_0, \mathbf{r}_0; \omega_0)\}\cdot\hat{\mathbf{n}}] \quad (1)$$

where $\mathbf{G}(\mathbf{r}_0,\mathbf{r}_0;\omega_0)$ is the Green's dyadic evaluated at the dipole location $\mathbf{r}_0$, and $\hat{\mathbf{n}}$ is a unit vector parallel to the emitter's transition dipole.[16] Note, for an NV center, eq 1 is further complicated by the presence of 2 orthogonal emission dipoles. Given that the diamond crystal can have a complicated and asymmetric shape, the position of the tip relative to the diamond crystal will determine the structure of the pLDOS probed by the NV center. Compared to an emitter without a host material, such as a single molecule, the diamond crystal adds considerable complications to interpreting the pLDOS measurement of an object.[8]

With an understanding of the near-field optical properties of the NV center, we next study the impact an optical antenna has on the NV center excited state dynamics. Figure 3a,b presents lifetime and intensity autocorrelation measurements on a single NV center with and without a proximal optical antenna (the top row in Figure 3 correspond to NV1/tip 1 and the bottom row are from NV2/tip 3). In Figure 3a,b, the tip reduces the NV center lifetime by a factor of ~3 (Figure 3a from 13 to 6 ns and Figure 3b from 30 to 9.6 ns). To demonstrate nanoscale FLIM, we exploited the NV center optical-transition lifetime as a probe of an optical antenna's nanoscale LDOS. The NV center is positioned in the confocal focus of the microscope. The Ag tip is then raster scanned through the focus and the lifetime is recorded for each $x-y$ location of the tip. By working with the modality illustrated in Figure 1a (bottom panel) we ensure the NV center far-field excitation conditions do not change. Figure 3c,e/d,f present simultaneously acquired FLIM and near-field images for the two crystal-tip combinations (NV1/tip 1 and NV2/tip 3; white circles indicate crystal boundary from topography). The insets in Figure 3c–f are linecuts along the indicated lines. The FLIM images were constructed by fitting the lifetime with a single exponential. We did not observe any biexponential behavior in the lifetime, and therefore, we do not think there was any fast switching between the two NV charged states (see Supporting Information Figure S5 for lifetime fits). Again, comparing Figure 3c and e we observe a localized hot spot in the FLIM (and near-field image) presented in Figure 3e (Figure 3f).

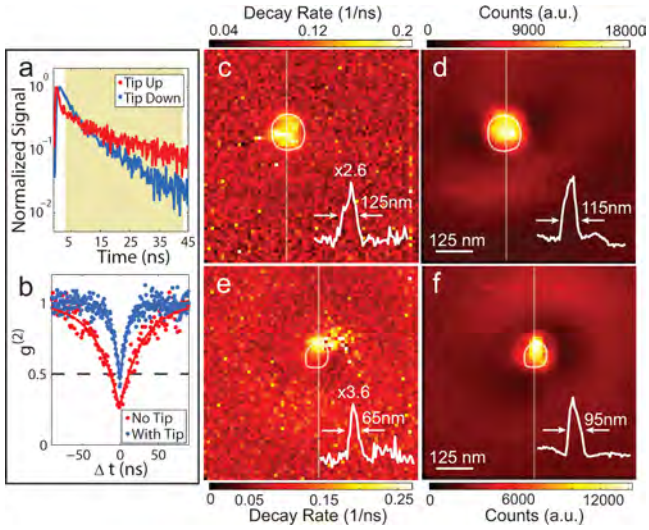

Figure 3. Fluorescence lifetime imaging microscopy (FLIM) with a single NV center. (a) Lifetime measurements for NV center 1 with and without tip 1. The presence of the tip reduces the NV center lifetime. The shaded region indicates the fitted region of the lifetime curve used in the FLIM image construction. (b) Intensity autocorrelation function for NV center 2 and a third Ag tip (tip 3). The measurement is made with and without the tip. There is no background correction. (c) Fluorescence lifetime image microscopy of tip 1 with NV center 1. The circle corresponds to the crystal topography. The inverse of lifetime is plotted (the decay rate). Inset: Linecut corresponding to the line indicated in the image. (d) The near-field fluorescence image taken concurrent to the FLIM image in panel c. Inset: Linecut corresponding to the line indicated in the image. (e) Fluorescence lifetime image microscopy of tip 3 with NV center 2. The circle corresponds to the crystal topography. The inverse of lifetime is plotted (the decay rate). Inset: Linecut corresponding to the line indicated in the image. (f) The near-field fluorescence image taken concurrent to the FLIM image in panel e. Inset: Linecut corresponding to the line indicated in the image.

dx.doi.org/10.1021/nl401791v | Nano Lett. 2013, 13, 3807–3811

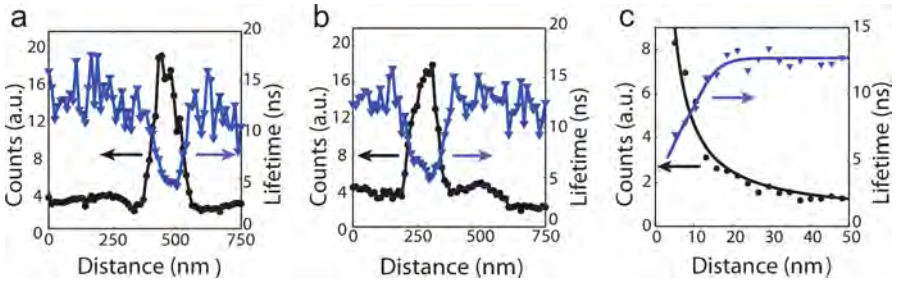

Figure 4. FLIM resolving power. (a) Near-field fluorescence count rates and corresponding lifetimes for an *x*-linecut through the images in Figure 3c,d. (b) Near-field fluorescence count rates and corresponding lifetimes for a *y*-linecut through the images in Figure 3c,d. (c) Near-field fluorescence count rates and corresponding lifetimes for an approach curve taken with NV 1 and tip 1. The solid lines are to guide the eye.

To illustrate the potential resolving power of the FLIM technique, Figure 4 presents *x*-, *y*-, and *z*-linecuts of both the FLIM and near-field image of Figure 3c,d (NV1/tip1). In the *x*-direction (*y*-direction) we find both approaches result in a full-width at half-maximum for the linecut of ∼100 nm (∼100 nm). We emphasize that the notion of resolution is complicated by the tip−crystal interaction, but one could imagine tailored nanocrystal geometries designed to exhibit responses that are better resolved than the length scale that characterizes the diamond crystal size. To complement the previous linecuts, a final data set was recorded as the tip was retracted from the diamond nanocrystal. The measured decay length in this instance was ∼10 nm. Combining the linecuts in the three perpendicular directions, the LDOS is probed in a volume corresponding to 100 × 100 × 10 nm^3. On the basis of the lack of fluorescence quenching in Figure 4c and in a previous near-field fluorescence study using pyramid tips,[39] we conclude that the observed fluorescence enhancement is a combination of the radiative rate increasing and more efficient excitation of the NV center (see the last section of Supporting Information for a further discussion of this point).

In conclusion, we have demonstrated that the NV center optical transition is a sensitive probe of the local electromagnetic mode structure. We observed an order of magnitude increase in the NV center fluorescence and measured reduction in lifetimes of ∼3. Additionally, the ability to resolve fluorescence from the NV center in the presence of an optical antenna suggests it should be possible to realize a scanning probe instrument to measure LDOS that affixes the diamond nanocrystal to the vertex of an optical antenna. However, the diamond nanocrystal introduces challenges in interpreting the LDOS measurements, due to the additional structure and inhomogeneity, discussed above, and the variations in quantum yield.[14,26] The attractiveness of the NV center for LDOS imaging is that it could be used simultaneously to measure local electric and magnetic fields realizing a probe that could provide a wealth of nanoscale information in the vicinity of either target nanophotonic devices or biological material.

■ ASSOCIATED CONTENT

Supporting Information

Details on maximum fluorescence enhancement, near-field signal dependence on tip position, near-field hot spots, lifetime linecuts of NV center 1 and Ag tip 1, lifetime fits, and saturation and decay rate. This material is available free of charge via the Internet at http://pubs.acs.org.

■ AUTHOR INFORMATION

Corresponding Author

*(A.N.V.) E-mail: nick.vamivakas@rochester.edu.

Notes

The authors declare no competing financial interest.

■ ACKNOWLEDGMENTS

We thank P. Bharadwaj, M. Frimmer, Z. Lapin, and L. Rondin for valuable input and advice. A.N.V. acknowledges support from the Institute of Optics. L.N. acknowledges support from the Department of Energy (DE- FG02-05ER46207). T.W.J. and S.-H.O. acknowledge support from the Office of Naval Research Young Investigator Award (N00014-11-1-0645) and the DARPA Young Faculty Award. Capital equipment available for this research was partially funded under Contract Number: W911NF0910425(N.George,PI) supported by Dr. Richard Hammond, Physics Division, U.S, Army Research Office.

■ REFERENCES

(1) Purcell, E. M. *Phys. Rev.* **1946**, *69*, 681.
(2) Drexhage, K. H. *J. Lumin.* **1970**, *1/2*, 693−701.
(3) Hulet, R. G.; Hilfer, E. S.; Kleppner, D. *Phys. Rev. Lett.* **1985**, *55*, 2137−2140.
(4) Anger, P.; Bharadwaj, P.; Novotny, L. *Phys. Rev. Lett.* **2006**, *96*, 113002.
(5) Schietinger, S.; Barth, M.; Aichele, T.; Benson, O. *Nano Lett.* **2009**, *9*, 1694−1698.
(6) Curto, A. G.; Volpe, G.; Taminiau, T. H.; Kreuzer, M. P.; Quidant, R.; van Hulst, N. F. *Science* **2010**, *329*, 930−933.
(7) Schell, A. W.; Kewes, G.; Hanke, T.; Leitenstorfer, A.; Bratschitsch, R.; Benson, O.; Aichele, T. *Opt. Express* **2011**, *19*, 7914−7920.
(8) Kühn, S.; Håkanson, U.; Rogobete, L.; Sandoghdar, V. *Phys. Rev. Lett.* **2006**, *97*, 017402.
(9) Farahani, J. N.; Pohl, D. W.; Eisler, H.-J.; Hecht, B. *Phys. Rev. Lett.* **2005**, *95*, 017402.
(10) Ropp, C.; Cummins, Z.; Nah, S.; Fourkas, J. T.; Shapiro, B.; Waks, E. *Nat. Commun.* **2013**, *4*, 1477.
(11) Yoshie, T.; Scherer, A.; Hendrickson, J.; Khitrova, G.; Gibbs, H. M.; Rupper, G.; Ell, C.; Shchekin, O. B.; Deppe, D. G. *Nature* **2004**, *432*, 200−203.
(12) Englund, D.; Shields, B.; Rivoire, K.; Hatami, F.; Vučković, J.; Park, H.; Lukin, M. D. *Nano Lett.* **2010**, *10*, 3922−3926.
(13) Geiselmann, M.; Juan, M. L.; Renger, J.; Say, J. M.; Brown, L. J.; Javier Garcia de Abajo, F.; Koppens, F.; Quidant, R. *Nat. Nanotechnol.* **2013**, *8*, 175−179.
(14) Frimmer, M.; Mohtashami, A.; Koenderink, A. F. *Appl. Phys. Lett.* **2013**, *102*, 121105.
(15) Tetienne, J.-P.; Rondin, L.; Spinicelli, P.; Chipaux, M.; Debuisschert, T.; Roch, J.-F.; Jacques, V. *New J. Phys.* **2012**, *14*, 103033.

(16) Novotny, L.; Hecht, B. *Principles of Nano-Optics*; Cambridge University Press: Cambridge, U.K., 2006.
(17) Henkel, C.; Sandoghdar, V. *Opt. Commun.* **1998**, *158*, 250−262.
(18) Rahmani, A.; Chaumet, P. C.; de Fornel, F.; Girard, C. *Phys. Rev. A* **1997**, *56*, 3245−3254.
(19) Michaelis, J.; Hettich, C.; Mlynek, J.; Sandoghdar, V. *Nature* **2000**, *405*, 325−328.
(20) Kühn, S.; Hettich, C.; Schmitt, C.; Poizat, J.-P.; Sandoghdar, V. *J. Microsc.* **2001**, *202*, 2−6.
(21) Sonnefraud, Y.; Chevalier, N.; Motte, J.-F.; Huant, S.; Reiss, P.; Bleuse, J.; Chandezon, F.; Burnett, M. T.; Ding, W.; Maier, S. A. *Opt. Express* **2006**, *14*, 10596−10602.
(22) Cuche, A.; Drezet, A.; Sonnefraud, Y.; Faklaris, O.; Treussart, F.; Roch, J.-F.; Huant, S. *Opt. Express* **2009**, *17*, 19969−19980.
(23) Frimmer, M.; Chen, Y.; Koenderink, A. F. *Phys. Rev. Lett.* **2011**, *107*, 123602.
(24) Hui, Y. Y.; Lu, Y.-C.; Su, L.-J.; Fang, C.-Y.; Hsu, J.-H.; Chang, H.-C. *Appl. Phys. Lett.* **2013**, *102*, 013102.
(25) Tisler, J.; Oeckinghaus, T.; Stöhr, R.; Kolesov, R.; Reinhard, F.; Wrachtrup, J. *arxiv: 1301.0218* **2013**.
(26) Mohtashami, A.; Koenderink, A. F. *New J. Phys.* **2013**, *15*, 043017.
(27) Wrachtrup, J.; Jelezko, F. *J. Phys.: Condens. Matter* **2006**, *18*, S807.
(28) Kurtsiefer, C.; Mayer, S.; Zarda, P.; Weinfurter, H. *Phys. Rev. Lett.* **2000**, *85*, 290−293.
(29) Brouri, R.; Beveratos, A.; Poizat, J.-P.; Grangier, P. *Opt. Lett.* **2000**, *25*, 1294−1296.
(30) Balasubramanian, G.; Chan, I. Y.; Kolesov, R.; Al-Hmoud, M.; Tisler, J.; Shin, C.; Kim, C.; Wojcik, A.; Hemmer, P. R.; Krueger, A.; Hanke, T.; Leitenstorfer, A.; Bratschitsch, R.; Jelezko, F.; Wrachtrup, J. *Nature* **2008**, *455*, 648−651.
(31) Maze, J. R.; Stanwix, P. L.; Hodges, J. S.; Hong, S.; Taylor, J. M.; Cappellaro, P.; Jiang, L.; Gurudev Dutt, M. V.; Togan, E.; Zibrov, A. S.; Yacoby, A.; Walsworth, R. L.; Lukin, M. D. *Nature* **2008**, *455*, 644−647.
(32) Maurer, P. C.; Maze, J. R.; Stanwix, P. L.; Jiang, L.; Gorshkov, A. V.; Zibrov, A. A.; Harke, B.; Hodges, J. S.; Zibrov, A. S.; Yacoby, A.; Twitchen, D.; Hell, S. W.; Walsworth, R. L.; Lukin, M. D. *Nat. Phys.* **2010**, *6*, 912−918.
(33) Dolde, F.; Fedder, H.; Doherty, M. W.; Nöbauer, T.; Rempp, F.; Balasubramanian, G.; Wolf, T.; Reinhard, F.; Hollenberg, L. C. L.; Jelezko, F.; Wrachtrup, J. *Nat. Phys.* **2011**, *7*, 459−463.
(34) Kolkowitz, S.; Bleszynski Jayich, A. C.; Unterreithmeier, Q. P.; Bennett, S. D.; Rabl, P.; Harris, J. G. E.; Lukin, M. D. *Science* **2012**, *335*, 1603−1606.
(35) Staudacher, T.; Shi, F.; Pezzagna, S.; Meijer, J.; Du, J.; Meriles, C. A.; Reinhard, F.; Wrachtrup, J. *Science* **2013**, *339*, 561−563.
(36) Mamin, H. J.; Kim, M.; Sherwood, M. H.; Rettner, C. T.; Ohno, K.; Awschalom, D. D.; Rugar, D. *Science* **2013**, *339*, 557−560.
(37) Tzeng, Y.-K.; Faklaris, O.; Chang, B.-M.; Kuo, Y.; Hsu, J.-H.; Chang, H.-C. *Angew. Chem., Int. Ed.* **2011**, *50*, 2262−2265.
(38) Bharadwaj, P.; Deutsch, B.; Novotny, L. *Adv. Opt. Photonics* **2009**, *1*, 438−483.
(39) Johnson, T. W.; Lapin, Z. J.; Beams, R.; Lindquist, N. C.; Rodrigo, S. G.; Novotny, L.; Oh, S.-H. *ACS Nano* **2012**, *6*, 9168−9174.
(40) Greffet, J.-J.; Hugonin, J.-. P.; Besbes, M.; Lai, N. D.; Treussart, F.; Roch, J.-. F. *arxiv: 1107.0502* **2011**.
(41) Han, K. Y.; Willig, K. I.; Rittweger, E.; Jelezko, F.; Eggeling, C.; Hell, S. W. *Nano Lett.* **2009**, *9*, 3323−3329.

Supporting information for: Nanoscale fluorescence lifetime imaging of an optical antenna with a single diamond NV center

Ryan Beams,[†] Dallas Smith,[†] Timothy W. Johnson,[‡] Sang-Hyun Oh,[‡] Lukas Novotny,[¶] and A. Nick Vamivakas[*,†]

Institute of Optics, University of Rochester, Rochester, New York 14627, USA, Department of Electrical and Computer Engineering, University of Minnesota, Minneapolis, Minnesota 55455, USA, and ETH Zürich, Photonics Laboratory, 8093 Zürich, Switzerland

E-mail: nick.vamivakas@rochester.edu

Maximum fluorescence enhancement

In the main text we report an average enhancement of 9.7 ± 2.6 for all NV centers studied. This average does not include the maximum fluorescence enhancement we observed of 17. The near-field image of the crystal exhibiting the maximum enhancement is presented in Figure 1a (the corresponding topography is in Figure 1b). The inset of Figure 1a is a linecut along the direction indicated. The enhancement is calculated by comparing the maximum confocal fluorescence counts with the maximum near-field counts. The 17 is a combination of excitation enhancement and increased radiative transition rate.

[*]To whom correspondence should be addressed

[†]Institute of Optics, University of Rochester, Rochester, New York 14627, USA

[‡]Department of Electrical and Computer Engineering, University of Minnesota, Minneapolis, Minnesota 55455, USA

[¶]ETH Zürich, Photonics Laboratory, 8093 Zürich, Switzerland

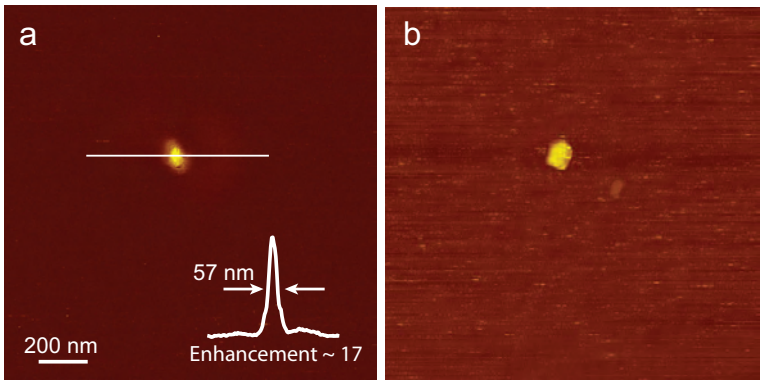

Figure 1: Fluorescence enhancement. (a) Near-field image of a diamond nanocrystal with NV center. The fluorescence enhancement is determined to be 17 from comparison with the confocal fluorescence image of the same NV center. Inset: Linecut indicated by the solid line in the near-field image. (b) Topography map taken simultaneously with the near-field image.

Near-field signal dependence on tip position

The structure of the near-field fluorescence signal was explored by acquiring repeated near-field images using the same tip and NV center while varying the alignment of the tip position in the focus. In Figure 2a the tip was positioned to the upper left of the focus and two lobes are clearly seen. When the tip is positioned just slightly to left of the focus, the near-field image is more uniform, but still has some structure, Figure 2b. Finally, in Figure 2c the tip is centered in the focus and the near-field pattern is uniform. The contrast in Figure 2a was scaled by a factor 3 compared to Figure 2b,c. The corresponding topography images are shown on the bottom row of Figure 2. Since all of these images were acquired using the same tip and NV center, the patterns cannot be caused by tip specific structure, such as a double tip.

Near-field hot spots

An example of a near-field image of another single NV center that exhibits hot spots is presented in Figure 3a. The curve in Figure 3a is the outline of the crystal boundary as determined from the topography map in Figure 3b. The near-field fluorescence is inhomogeneously distributed with respect to the diamond nanocrystal.

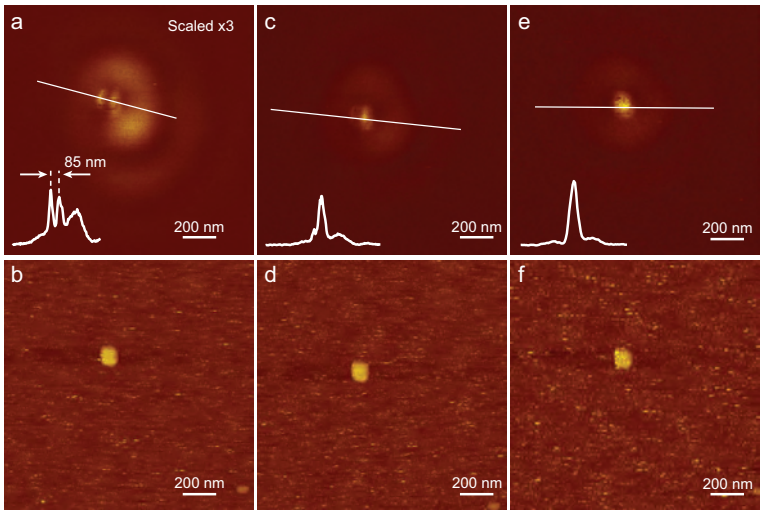

Figure 2: Near-field optical image of a single nitrogen vacancy for different alignments of the Ag pyramid tip in the optical focus. The top row shows the near-field fluorescence images with the tip positioned to the (a) upper left, (b) slightly to the left, and (c) in the center of the focus. The contrast in (a) has been scaled by a factor 3. (d), (e), (f) The topography for each image is shown on the bottom row. The insets show the linecuts across the images and are scaled the same.

Lifetime linecuts of NV center 1 and Ag tip 1

The crystal discussed in Figure 2f in the main text exhibits localized hot-spots in the near-field image. In Figure 4a we present a second near-field image of NV center 1 with tip 2 from the manuscript. Linescans were acquired along the white lines by keeping the tip in the focus and scanning the sample, opposed to scanning the tip over the sample as in Figure 3 of the main text. At each location, the lifetime was measured as well as the total counts, shown in Figure 4(b)-(d).

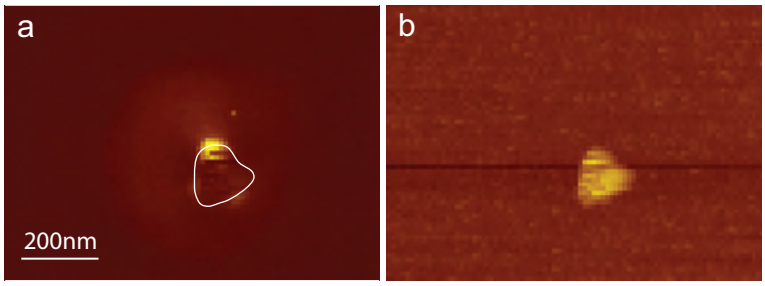

Figure 3: Near-field fluorescence hot spots. (a) Near-field fluorescence image of an NV center. (b) The topography map of the diamond nanocrystal.

The short lifetime away from the particle, ~ 2 nm, is from the glass and Ag tip. Comparing the lifetime to the total counts shows that increased fluorescent counts are accompanied by a lifetime change (vertical dashed line).

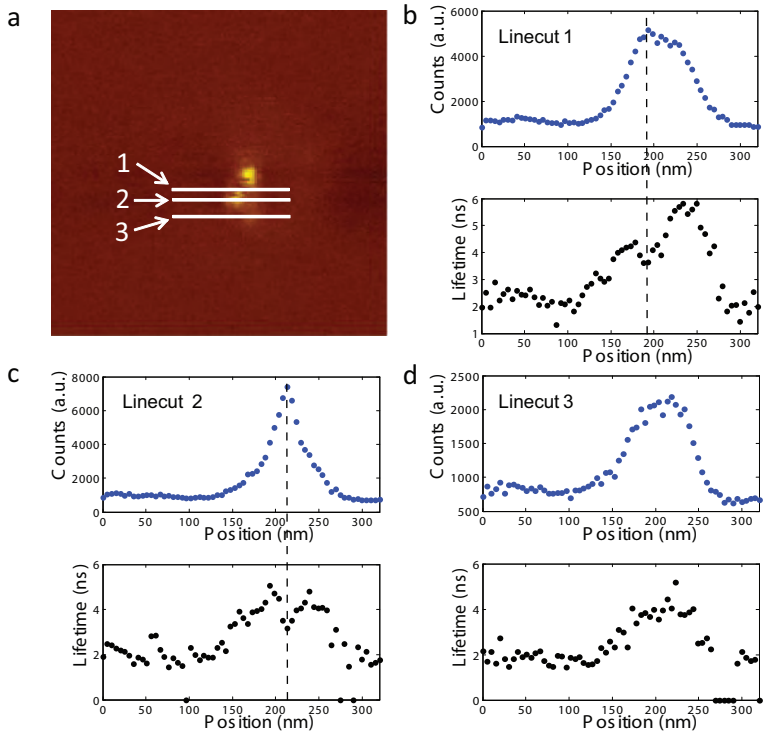

Figure 4: Fluorescence lifetime linecuts. (a) Near-field image of the NV center in Figure 2f and 2g. The solid lines indicate the linecuts presented in panels S4b-S4d. (b) Near-field fluorescence and lifetime for the linecut indicated in Figure S4a. Same for (c) and (d).

Lifetime fits

Figure 5 show example lifetime curves taken from the retract curve in Figure 4c from the main text. The lifetime with the tip down (Figure 5(a)) and retracted (Figure 5(b)) are shown. Both curves are fit with a single exponential. These curves illustrate the lifetime change as well as the increase in counts due to the presents of the tip.

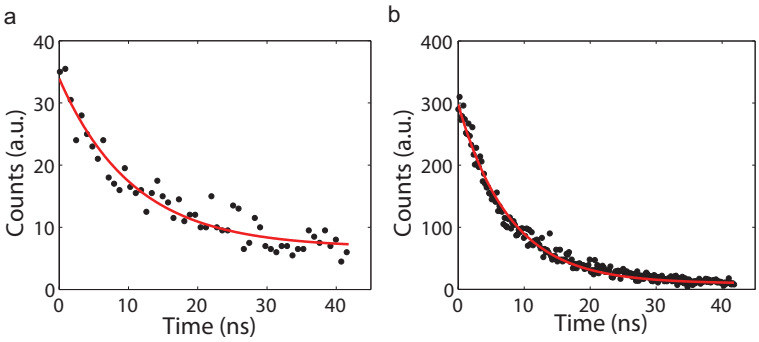

Figure 5: Lifetime curves of an NV center with single exponential fit with (a) the tip retracted and (b) the tip landed.

Saturation and decay rate

Figure 6(a) shows a saturation curve for an NV center using linear cw excitation with the glass background subtracted. The arrow indicates 30 μW, which was used for the FLIM images. For the near field images presented in the manuscript, an excitation power of 10 to 30 μW was used. The FLIM images were taken using 30 μW of excitation power. While this is a far-field measurement, it can be used to get an upper bound on the NV saturation with a tip. The typically enhancements we observed were $\sim$10. If all of the enhancement was due to field localization of the antenna, then the excitation power in the presence of the tip would be 150 μW (300 μW) for the near-field (FLIM) images. From Figure 6(a), 150 μW is in the linear regime and 300 μW, while no longer linear, is below saturation.

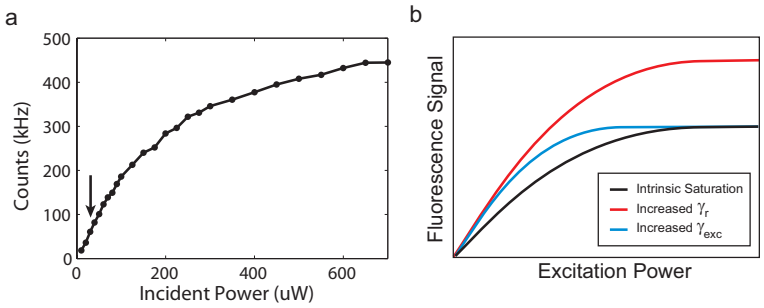

Figure 6: (a) Saturation curve using linear power without a tip. The arrow indicates the power used for the FLIM measurements (30 μW). (b) Sketches of the saturation changes if the radiative rate (red), γ_r, or the excitation rate (blue), γ_{exc}, is increased.

This upper limit assumes that the tip does not increase the out-coupling efficiency or change the decay rate of the NV center. The FLIM measurements clearly show that the excited state dynamics are influenced by the presence of the tip. However, the near-field enhancement is not solely due to a change in the excitation rate, since the observed lifetime changes were ≈ 3. Based on the enhancement observed using pyramid tips in Ref. [36], we expect the lifetime change to be predominately due to the radiative rate increasing, γ_r. This is can also be seen by the absence of quenching in Figure 5c in the manuscript.

Using Ref. [5], the fluorescence rate, γ_{em} is defined as,

$$\gamma_{em} = \gamma_{exc} \frac{\gamma_r}{\gamma}, \tag{1}$$

where γ is the total decay rate and γ_{exc} is the excitation rate. Figure 6(b) shows sketches of the change to the intrinsic saturation curve (black) if γ_r (red) or γ_{exc} (blue) are changed. In the data shown in the main text, both γ_r and γ_{exc} are increased due to the presence of the tip.